Solid State Phenomena Vols 156-158 (2010) pp 223-228 *Online: 2009-10-28*
© (2010) Trans Tech Publications, Switzerland
doi:10.4028/www.scientific.net/SSP.156-158.223

Simulation of Iron Distribution after Crystallization of mc Silicon

J. Schön[1,2,a], H. Habenicht[1,b] , M.C. Schubert[1,c] and W. Warta[1,d]

[1]Fraunhofer Institute for Solar Energy Systems (ISE), Heidenhofstr. 2, 79110 Freiburg, Germany

[2]University of Freiburg, Material Research Center, Stefan-Meier-Str. 21, 79104 Freiburg, Germany

[a]jonas.schoen@ise.fraunhofer.de, [b]holger.habenicht.schoen@ise.fraunhofer.de,
[c]martin.schubert@ise.fraunhofer.de, [d]wilhelm.warta@ise.fraunhofer.de

Keywords: Simulation, gettering, iron, precipitation

Abstract. Interstitial iron (Fe_i) and iron-boron pairs influence or even limit the recombination lifetime in industrial block cast multicrystalline (mc) silicon, though the proportions in the total iron concentration are generally small. Most of the iron in mc silicon is precipitated and less recombination active. This work aims for a better understanding of the distribution of iron in its different states (precipitated or dissolved) over the block height, as well as in regions of different crystal quality. In experimental studies several features of iron in mc silicon were observed, which occur due to the high extended defect density. In our 2-dimensional model for mc silicon, trapping of interstitial Fe at extended defects and precipitation at the extended defects are taken into account. The results are compared with NAA-data and spatial resolved measurements of the Fe_i concentration.

Introduction

The behavior of impurities near grain boundaries and dislocations are determined by a combination of two mechanisms: (1) segregation, i.e. increased equilibrium metal solubility due to local distortion of the lattice and (2) relaxation, i.e. precipitation of supersaturated impurities at extended defects during cooling down [1,2]. Together the two mechanisms lead to a higher concentration of iron in regions with high extended defect concentration, especially for long cooling times which are typical during block cast solidification of mc silicon (>20 hours). The resistance to external gettering of impurities in regions with a high dislocation density, which was shown in several experiments, can be explained with an efficient internal gettering by the extended defects. Istratov et al [1] attempted to quantitatively separate the two effects and found segregation coefficients of 2.2 - 16 for iron between polysilicon and non-disturbed CZ silicon at temperatures of 1150°C and 1000°C. The existing theoretical models for the interactions of impurities with dislocations are not able to explain the observed interaction at high temperature [3].

Modeling internal gettering of iron in mc silicon

In [4] we showed that the Sentaurus® platform [5] could be used to model external and internal gettering of iron with a homogeneous defect density. We used the precipitation model for monocrystalline silicon by Haarahiltunen et al [6], based on the Fokker Planck Equation (FPE). Transferring the FPE-model for monocrystalline silicon to the mc case, one has to slightly modify the equations. Following the argumentation of Ham [7] for extended defects, one could express the growth and the dissolution rates as:

$$g(n,t) = \frac{2\pi l_p D\ \mathrm{Fe_i}}{-\ln(r\sqrt{\pi \mathrm{DL}}) - 3/5} \quad ; \qquad d(n,t) = \frac{2\pi l_p D}{-\ln(r\sqrt{\pi \mathrm{DL}}) - 3/5} C_{Sol}\, e^{\left(\frac{E_a}{kT\sqrt{n}}\right)} \quad (1)$$

These rates appear in the evolution of the size distribution of precipitates (for details see [6])

$$\frac{\partial f(n,t)}{\partial t} = \frac{\partial}{\partial n}\left\{-[g(n,t) - d(n,t)]f(n,t) + \frac{[g(n,t) + d(n,t)]}{2}\frac{\partial f(n,t)}{\partial n}\right\} . \quad (2)$$

DL is the dislocation density, l_p = 2.7·10^{-8} cm the possible precipitation center density along the dislocation and r the radius of the dislocation core, which was assumed to be 1 nm. Fe_i denotes the interstitial iron concentration, D the diffusivity and n the number of iron atoms in a precipitate. For the fitting parameter E_a, which includes surface as well as morphology effects, the well proven values (1.015·10^{-4}·T+0.8033) eV for T<773K and (6.038·10^{-4}·T+0.4150) eV for T≥773K [6] were chosen. The solubility of iron near the interface of a large precipitate below the eutectic temperature is represented by $C_{Sol(\mathrm{mono})}$=4.3·10^{22}·exp(-2.1/kT) cm^{-3} [8]. Above the eutectic temperature we use a maximum Fe solubility of 1.5·10^{16} cm^{-3} derived from the few existing data [9]. The number of possible precipitation sites is given by N_0 =DL/l_p. The parameter P_1 = 2·10^5 adjusted the density of precipitation sites occupied with one Fe atom

$$f(1,t) = P_1 f(0,t)\exp\left(\frac{kT\ln(\mathrm{Fe_i}/C_{Sol}) - 2E_a}{kT}\right) \tag{3}$$

.

Simplifying and interpreting grain boundaries as strings of dislocations, we focus on dislocations (DL) as trapping centers for impurities. The Fe solubility in the presence of trapping at DL becomes:

$$C_{Sol} = C_{Sol(\mathrm{mono})}\,(1+C_1\cdot \mathrm{DL})\,. \tag{4}$$

In the framework of the SolarFocus project mc silicon ingots were intentionally contaminated with iron. The total metal concentrations over block height were determined with Neutron Activating Analyses (NAA). We obtained the effective segregation coefficient k_S between melt and solid mc silicon by modeling the metal distribution as a function of fraction solidified f_S with the Scheil equation $C(x) = C_0\cdot(1-f_S)^{(k_s-1)}$ [10]. The Scheil equation gives a good approximation of the impurity distribution in solidified material well below the top, if the impurity concentration is homogenous in the melt and if diffusion in the solid can be neglected. For iron we found an effective segregation coefficient of 2.2·10^{-5} for the intentionally contaminated ingots, which is 3-4 times higher than the literature data for monocrystalline silicon $k_{S(\mathrm{mono})}$=5-7·10^{-6} [11,12]. Kvande et al. [13] achieved in similar experiments a segregation coefficient of 2.0·10^{-5} and found an interstitial Fe_i concentration around 1·10^{13} cm^{-3} in the middle of the ingot for 1.3·10^{18} cm^{-3} initial Fe concentration.
Assuming that the higher proportion of Fe in the solid mc silicon is due to interaction of Fe with the extended defects, the solid solubility in highly dislocated regions is obtained. Expressing the segregation coefficient between low and high dislocated regions as $k_{\mathrm{DL}} = C_{Sol(\text{high DL})} / C_{Sol(\mathrm{mono})}$ and extract C_1 in Eq. 4 for the temperature of solidification, we get C_1=8.92·10^{-7}eVcm^{-3}/kT.

2D model based on EPD

A crucial parameter for the precipitation of iron is the DL density. Two measurement techniques were used to determine the DL density of the intentionally contaminated ingots. The etch pit density (EPD) of selected samples from a medium height of the ingot were measured by counting the etched silicon defects microscopically. Because an EPD measurement of the whole wafer would be too time-consuming, we used an image of a 10 cm x 10 cm wafer, parallel to the EPD samples to approximate the proportion of highly dislocated regions. Single etch pits are not detectible with this method, but accumulations of etch pits could be seen as black dots.
Fig. 1 shows the secco-etched wafer and details of the EPD measurements on parallel wafers. In an area with high DL density we found that 53 % of the area has an EPD above 10^6 cm^{-2}, 32% between 10^5 cm^{-2} and 10^6 cm^{-2} and only 15% below 10^5 cm^{-2}. The simple image of this area is about 21% black, whereas we found only 3.9% black areas over the whole wafer. Since the proportion of black in the areas with low EPD are less than 1%, one can easily calculate that 9.9% of the wafer has a DL

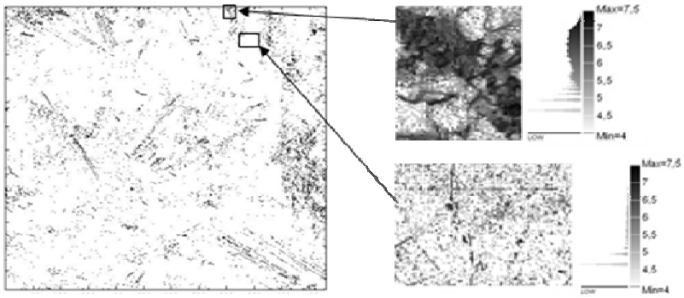

Figure 1: Image of a secco etched wafer 8.5 cm above the bottom and details of the EPD measurements with $1.3 \cdot 10^6$ cm^{-2} (top right, size 2.5 mm x 3.5 mm) and $1 \cdot 10^5$ cm^{-2} (bottom right, size: 4.6 mm x 3.1 mm) mean EPD.

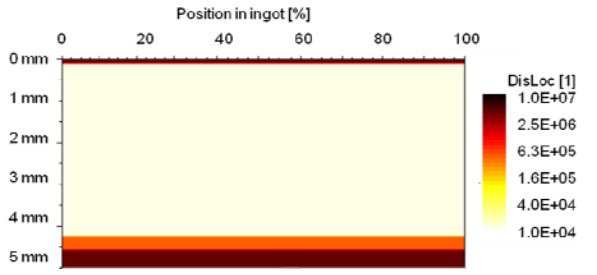

Figure 2: The dislocation (DL) structure used in the simulation. Four different DL areas ($4 \cdot 10^6$, $1 \cdot 10^4$, $4 \cdot 10^5$ and again $4 \cdot 10^6$cm^{-2}) are vertical homogenous from the bottom of the ingot (left side) to the top (right).

density higher than 10^6 cm^{-2}. Furthermore we found a mean value of $4 \cdot 10^6$ cm^{-2} for the high EPD, $4 \cdot 10^5$ cm^{-2} for the intermediate EPD and below $1 \cdot 10^4$ cm^{-2} for the group with low EPD. This is only a rough estimate, but we will see that moderate variations of the DL density or area size have only a slight affect on the simulation of the Fe_i distribution.

The EPD data and the DL image were used to create a representative simple 2D structure (Fig.2), assuming that the mean DL density is the same in different ingot heights. Using typical sizes, the 2D structure consists of an area with low DL density representing a medium sized grain (diameter 4.2 mm), a grain boundary on one side and a small medium dislocated grain, followed by a highly dislocated area on the other side. Back-diffusion during cooling down and the in-diffusion from the crucible is taken into account for comparison of the final metal concentration with NAA measurements. At the bottom we simulate the segregation from the crucible with an initial Fe contamination of $1.5 \cdot 10^{18}$ cm^{-3} which is in the range of measured data [14]. Three different temperature profiles (bottom, middle, top) modeled by Access e.V. were used in the simulations.

Simulations of the total iron distribution

The simulation and the experimental results for an ingot with a contamination of $1 \cdot 10^{18}$ cm^{-3} Fe is shown in Fig. 3 (a) and 3 (b). One can see a high concentration of Fe near the bottom of the ingot (left side of the picture), where Fe diffuses in from the crucible. Through the top of the ingot (right) the total Fe concentration raises and a good correlation between simulated and measured

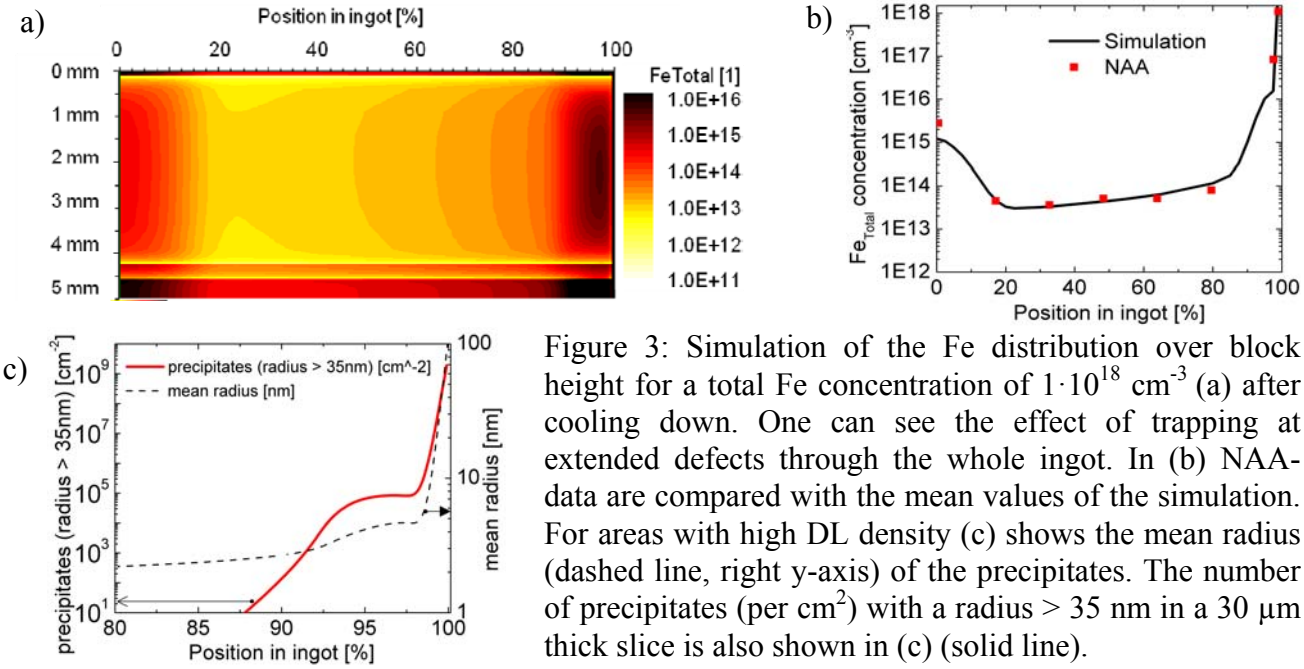

Figure 3: Simulation of the Fe distribution over block height for a total Fe concentration of $1 \cdot 10^{18}$ cm^{-3} (a) after cooling down. One can see the effect of trapping at extended defects through the whole ingot. In (b) NAA-data are compared with the mean values of the simulation. For areas with high DL density (c) shows the mean radius (dashed line, right y-axis) of the precipitates. The number of precipitates (per cm^2) with a radius > 35 nm in a 30 µm thick slice is also shown in (c) (solid line).

concentration is obtained (Fig. 3(b)). The segregation coefficient between a good grain and areas with high EPD is 24 at solidification temperature and around 33 at 900 C (Eq. 4), where the precipitation rate is high. Thus the segregation alone cannot explain the differences of more than 2 orders between the Fe concentrations in different areas. In addition, precipitation at the extended defects occurs during cooling down, which result in an effective metal flux to the extended defects, forming a denuded zone nearby on both sides of the grain. The simulation of the mean radius (Fig. 3(c)), assuming spherical precipitates, and the number of large precipitates (>35nm) indicate the amount of precipitates detectable by synchrotron measurements. From our simulation we expect that precipitates should be detectable within the upmost 7% of the ingot.

Simulations of the interstitial iron distribution

Recently developed techniques for spatial resolved measurements of the interstitial iron density [15, 16] allow a Fe_i-imaging of silicon wafers. The basics behind this technique are the different SRH-lifetime dependencies of Fe_i and iron-boron-pairs. From the difference in lifetime of two measurements, one performed after storage in the dark, where FeB pairs were formed, and one after light soaking, i.e. after splitting of the FeB pairs, the Fe_i concentration could be calculated [15].
The simulation for the ingot contaminated with $1 \cdot 10^{18}$ cm^{-3} Fe results in a noticeable proportion of precipitated Fe in low dislocated areas also for medium heights ($2\text{-}5 \cdot 10^{12}$ cm^{-3}). However the simulation of the Fe_i distribution (Fig. 4 (a)) exhibits that most of the Fe in low dislocated grains is in the interstitial state. In contrast the Fe_i concentrations in areas of high DL density do not significantly depend on the contamination level. This leads to a remarkable higher Fe_i concentration in lowly dislocated grains than in the adjacent grain boundaries with high DL density. The Fe_i image (Fig. 4 (b)) of a wafer (at 34% ingot height) shows a high contrast between grains and grain boundaries, too. Despite of this qualitative consistency between Fe_i image and simulation, the simulated Fe_i density in the grain of $6 \cdot 10^{12}$ cm^{-3} is higher than the measured $\sim 2\text{-}4 \cdot 10^{12}$ cm^{-3}. The mean Fe_i values of our Fe_i imaging are less than half of our Quasi-Steady-State-Photo-Conductive (QSSPC) measurements, a discrepancy which may be explained with a beginning dissociation of the FeB pairs during the Fe_i imaging measurement. The above mentioned QSSPC results [13] support our simulation, although they are slightly above our results. The difference in the Fe_i concentration is explained with the 1.3 times higher initial Fe concentration and a faster cooling down in [13].
In Fig. 5(a) a Fe_i concentration image of a wafer close to the bottom (8%) of an ingot contaminated with $1 \cdot 10^{17}$ cm^{-3} Fe is shown. Grain boundaries and grains with high DL density have a remarkable lower Fe_i concentration than good grains. The corresponding simulation (Fig. 5(d)) has the same characteristic, i.e. a drastically reduced Fe_i concentration in areas with high or medium DL density. This effect is weakened in the Fe_i image of a wafer with medium ingot position (Fig. 5(b)) and in consistency with the measurements the simulation shows only a small denuded zone near the high DL areas. The higher Fe_i concentration in a 1.5cm stripe at the right side of Fig. 5(b) is due to the in-diffusion from the edge of the ingot 2.5 cm right from the wafer and correspond well with simulation (width of the in-diffusion zone 3.9 cm). The Fe_i image from the top of the ingot (89% height) in Fig. 5(c) shows a substantial higher Fe_i concentration in large grains and a smaller overall

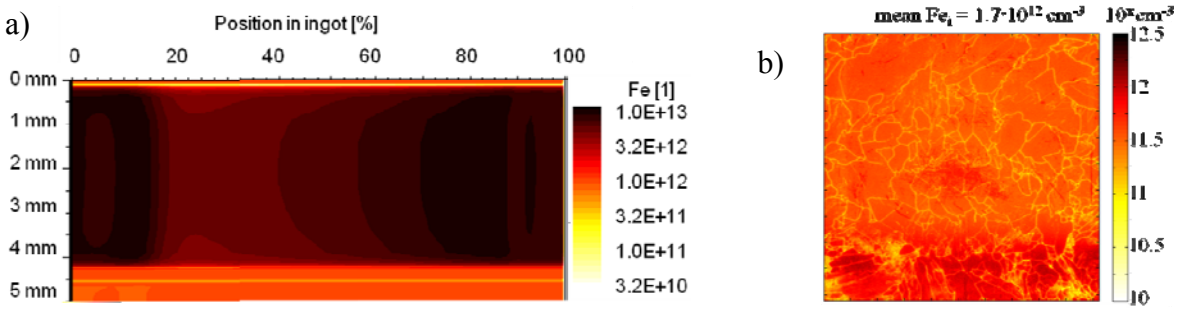

Figure 4: Simulated (a) and measured Fe_i (b) concentration after cooling down for an ingot intentionally contaminated with $1 \cdot 10^{18}$ cm^{-3} Fe.

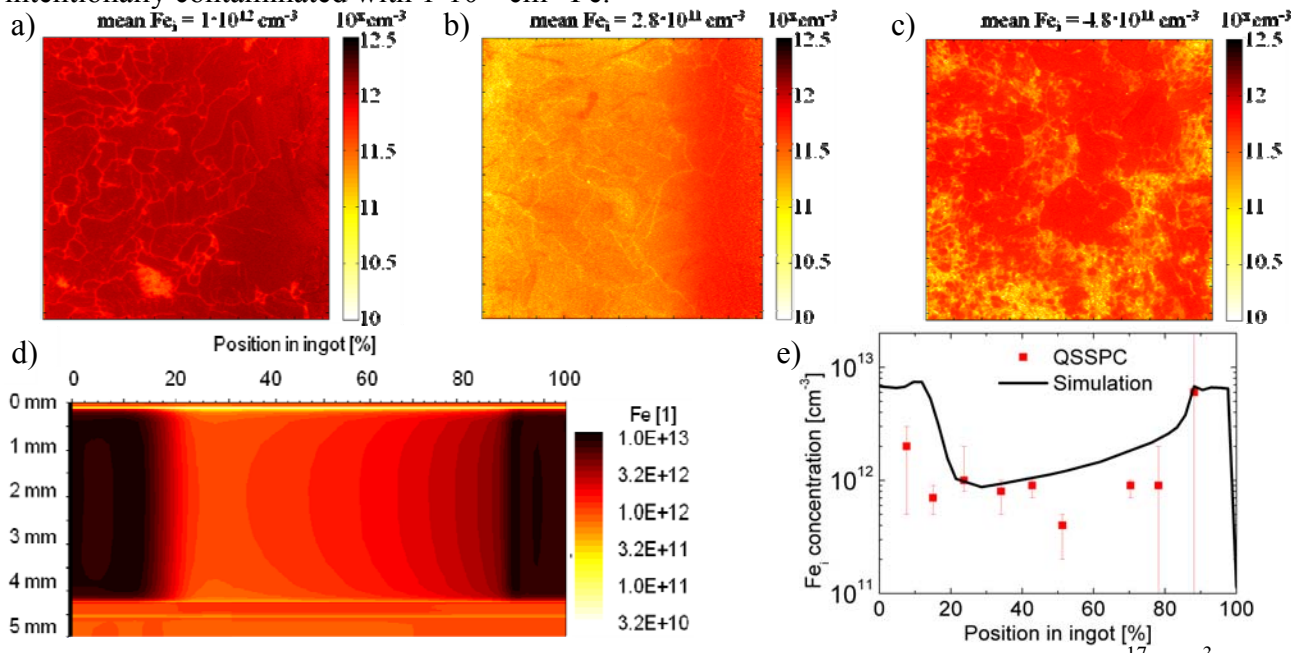

Figure 5: Simulation of the interstitial Fe density for the ingot contaminated with $1 \cdot 10^{17}$ cm^{-3} (d) in comparison with QSSPC measurements of the mean Fe_i concentration (e) and spatial resolved Fe_i images (5cm x 5cm) from different positions in the ingot (a) – (c).

Fe_i concentration compared to the bottom. Fe_i concentration compared to the bottom. The visible higher DL density is not considered in the simulation, but the qualitative results from Fig. 5(c) could be reproduced. In Fig. 5(e) the simulation of the Fe_i is compared with QSSPC data. Differences between simulation and QSSPC measurements are explained with the relatively high error due to the trapping effect in the top and the bottom of the ingot and the not representative DL density in the QSSPC spot size. The trapping effect in low lifetime areas does not appear in the Fe_i images. But also in these Fe_i images a part of the FeB pairs could be dissociated during measuring.
For a moderate total Fe concentration (below $5 \cdot 10^{13}$ cm^{-3}) the proportion of precipitated Fe in low dislocated grains is small and thus the higher total Fe concentration leads to higher Fe_i concentration. By contrast the Fe_i concentration in the moderately and highly dislocated areas is determined by the temperature at which the precipitation rate slows down. The precipitation is triggered by supersaturation of Fe_i, which is reduced near the DL because of higher solubility. Nevertheless most of the Fe precipitates in areas with high DL density, which could be explained by a higher precipitation core density and the increasing growth rate $\sim D \cdot k$(DL) (Eq. 1). A similar explanation was given by Haarahiltunen et al. for boron gettering [17].
For the reference ingot we estimated an overall Fe concentration of $3 \cdot 10^{16}$ cm^{-3}. The simulation of Fe_i distribution after cooling down and the comparison with the measurements is shown in Fig. 6. In areas with high DL density and an ingot position between 20% – 80% the segregation effect is higher than the precipitation rate. Therefore grains have a lower Fe_i concentration compared to the adjacent grain boundaries and other extended defects. The Fe_i image of a wafer from medium height

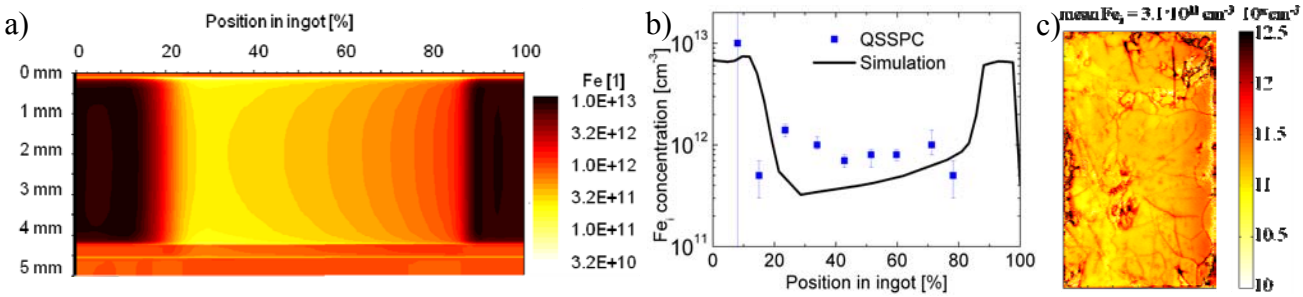

Figure 6: Fe_i distribution for a reference ingot. In contrast to the intentionally contaminated ingots the simulated (a) and measured (c) Fe_i concentrations are lower in grains than in grain boundaries. The Fe_i concentrations measured by QSSPC are slightly higher than the mean simulated values (b). (Fig. 6(c)) confirmed this simulation result. Most of the QSSPC results lie above (Fig. 6(b)), whereas the mean value of the Fe_i image is below the simulated results. A QSSPC spot size too close to the edge of the ingot could be a reason for the higher level of the measured Fe_i.

Conclusions and Outlook

A model of Fe distribution in mc silicon has been implemented in Sentaurus Process, taking segregation to high dislocated regions and precipitation at extended defects into account. Simulations of the Fe diffusion and accumulation at extended defects after solidification of mc silicon were compared to experimental results. The interstitial and total Fe concentrations over block height correspond well with experimental results. Important characteristics of Fe_i images like the denuded zones in the top and in the bottom of an ingot and the inversion in low contaminated silicon can be reproduced by the simulations.

We have now first results of 2D simulation of internal gettering in mc silicon. In further work one could use the model to define an as-cut state and combine the internal gettering with existing external gettering models, i.e. aluminum and phosphorus diffusion gettering. The temperature dependency of the segregation to the extended defects could be validated and optimized with experimental data of additional oxidation steps.

Acknowledgements

This work has been supported by the German Ministry for the Environment, Nature Conservation and Nuclear Safety under contract no. 0327650E (SolarFocus). The authors thank H. Behnken from Access e.V. for the temperature profiles.

References

[1] A.A. Istratov, et al., Proc. 14th. NREL Workshop (2004), p. 230.
[2] D. Macdonald, et al., J. Appl. Phys. 103, (2008) 073710.
[3] K. Sumino, Phys. stat. sol. (a) 171 (1999), p. 111.
[4] J. Schön, et al., 23rd EUPVSEC, Valencia, Spain (2008), p. 1851.
[5] Information on http://www.synopsys.com
[6] A. Haarahiltunen, et al., J. Appl. Phys. 101 (2007) 043507/1.
[7] F.S. Ham, Journal Phys. Chem. Solids 6 (1958) 335.
[8] M. Aoki and A. Hara, J. Appl. Phys. 74, (1993) 1440.
[9] E.R. Weber, Applied Physics A (Solids and Surfaces) A30 (1983) 1.
[10] E. Scheil, Z. Metallk. 34, (1942) 70.
[11] J. R. Davis, et al., IEEE Trans. Electron Devices 27, (1980) 677.
[12] H. Lemke, in *Semiconductor Silicon/1994*, edited by H. R. Huff et al, The Electrochemical Society, New Jersey, (1994), p.695.
[13] R. Kvande, et al., J. Appl. Phys. 104 (2008) 064905.
[14] E.Olsen, et al., Prog. Photovolt: Res. Appl. 16 (2008) 93-100.
[15] D. Macdonald, et al., J. Appl. Phys. 97, (2005) 033523.
[16] S. Herlufsen, et al., Phys. Stat. Sol. (RRL), (2008) p.1-3.
[17] A. Haarahiltunen, et al., Appl. Phys. Lett 92 (2008) 021902.

Gettering and Defect Engineering in Semiconductor Technology XIII
10.4028/www.scientific.net/SSP.156-158

Simulation of Iron Distribution after Crystallization of mc Silicon
10.4028/www.scientific.net/SSP.156-158.223

DOI References
[6] A. Haarahiltunen, et al., J. Appl. Phys. 101 (2007) 043507/1.
doi:10.1063/1.2472271
[7] F.S. Ham, Journal Phys. Chem. Solids 6 (1958) 335.
doi:10.1016/0022-3697(58)90053-2
[9] E.R. Weber, Applied Physics A (Solids and Surfaces) A30 (1983) 1.
doi:10.1007/BF00617708
[16] S. Herlufsen, et al., Phys. Stat. Sol. (RRL), (2008) p.1-3.
doi:10.1002/pssr.200802192